International Journal of Nanomedicine Dovepress

Open Access Full Text Article ORIGINAL RESEARCH

An Innovative Delivery System of Oxygen-Releasing Nanospheres and Self-Healing Hydrogels Enhances the Therapeutic Effectiveness of Bone Marrow Mesenchymal Stem Cells for Chronic Limb-Threatening Ischemia

Moyan Zhao[1], Zixuan Zhou[2], Amir Sherchan[1], Weizhong Yuan[2], Xiaoyun Xie[3], Maoquan Li[1,3]

[1]Shanghai Tenth People's Hospital, School of Medicine, Tongji University, Shanghai, 200092, People's Republic of China; [2]Key Laboratory of Advanced Civil Materials of Ministry of Education, School of Materials Science and Engineering, Tongji University, Shanghai, 201804, People's Republic of China; [3]Department of Intervention and Vascular Surgery, Shanghai Tenth People's Hospital, Shanghai, 200092, People's Republic of China

Correspondence: Maoquan Li, Department of Intervention and Vascular Surgery, Shanghai Tenth People's Hospital, Shanghai, 200092, People's Republic of China, Email cjr.limaoquan@vip.163.com

Purpose: Bone marrow mesenchymal stem cells (BMSCs) have emerged as promising candidate for postoperative therapeutics in chronic limb-threatening ischemia (CLTI). Nevertheless, their effectiveness is limited by their low survival rate and impaired functionality in the ischemic microenvironment. To overcome these challenges, we have devised an innovative delivery approach to support the utilization of BMSCs in CLTI therapy.

Methods: We synthesized oxygen-releasing nanospheres and self-healing hydrogels. The in vivo functionality of the hydrogel-nanosphere delivery system was evaluated via a multimodality animal live imaging system. A unilateral lower limb ischemia model was established in mice, and a delivery system loaded with BMSCs was administered. The experimental groups included normal mice, ischemic mice, ischemic mice treated with BMSCs in PBS, and ischemic mice treated with BMSCs in the delivery system. Blood perfusion was quantitatively measured via a laser doppler flowmeter (LDF). Immunofluorescence, Masson's trichrome staining, immunohistochemistry and enzyme-linked immunosorbent assay (ELISA) were also used.

Results: For cell viability analysis 80 $\mu g.mL^{-1}$ was considered the optimal concentration for cell survival. In vivo, 18 days after injection, the cell membrane fluorescence signal in the delivery system was significantly greater ($5.655^{10}\pm8.226^{8}$) p/s/cm²/sr than that in the other groups (p=0.043). Ischemic mice treated with BMSCs in the delivery system presented an improved limb salvage rate (0.926±0.12)% compared with that of ischemic mice treated with BMSCs in PBS (0.841±0.029)% at the 5th week after ischemia establishment (p=0.0033).

Conclusion: Our findings suggest that the survival time of BMSCs is prolonged in this innovative delivery system. The combination of nanospheres and hydrogels effectively restored vascular blood perfusion while exerting minimal toxicity on BMSCs. This novel approach combining oxygen-releasing nanospheres and self-healing hydrogels as a delivery system represents an advancement in enhancing the functionality of BMSCs to treat CLTI.

Keywords: nanoscale microsphere, stem cell therapy, delivery system, chronic vascular disease, revascularization, tissue recovery

Introduction

Chronic limb-threatening ischemia (CLTI) is a serious vascular condition characterized by significantly reduced blood supply to the extremities,[1] leading to tissue hypoxia, persistent pain, ulceration, and in severe cases, amputation.[2–4] Medication is often ineffective because of the lack of blood perfusion,[5] and approximately 50% of patients with subpatellar lesions do not meet the criteria for surgical revascularization.[6,7] Research on various innovative treatments

Received: 14 August 2024
Accepted: 10 November 2024
Published: 19 November 2024

Graphical Abstract

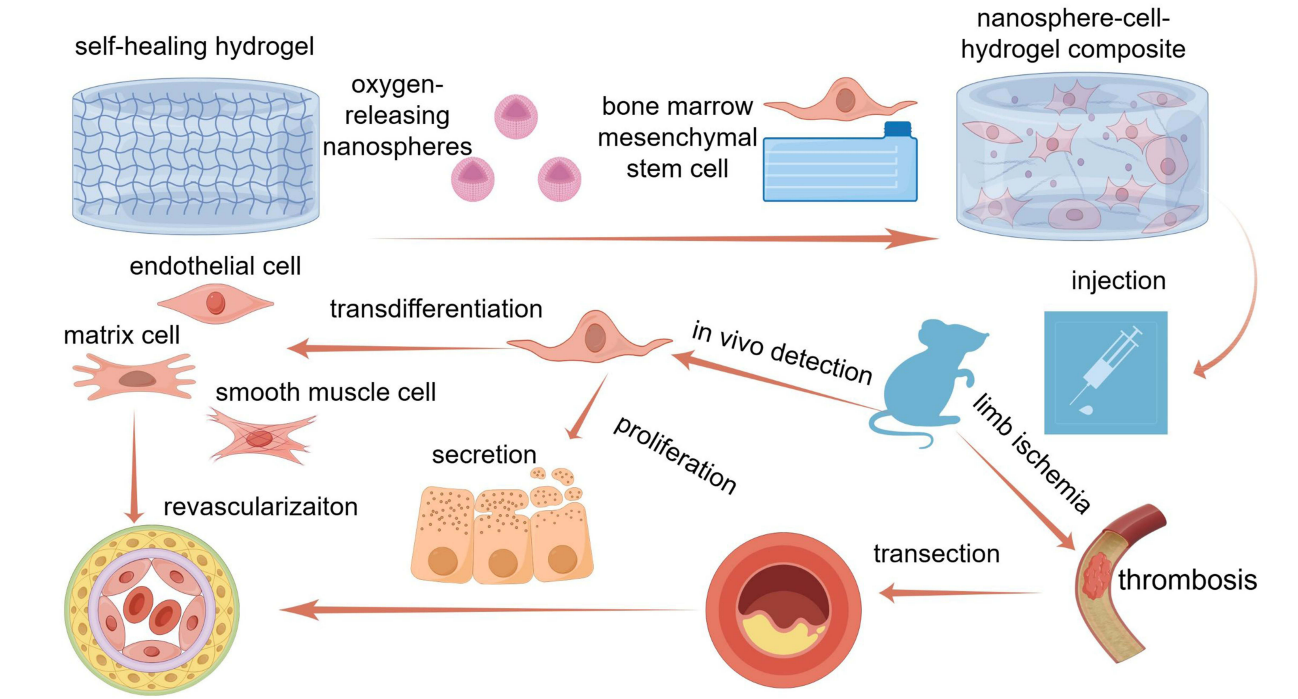

aimed at restoring blood flow to affected tissues, including angiogenesis therapy, stem cell therapy, gene therapy, hyperbaric oxygen therapy and nanomedicine is ongoing.[8] The use of nanoparticles to deliver drugs directly to ischemic tissues can improve drug efficacy and reduce side effects. Stem cell therapy has advantages in terms of tissue recovery,[9,10] with mesenchymal stem cells (MSCs) facilitating the development of collateral circulation in ischemic arteries,[11] thereby alleviating ischemic symptoms and decreasing the risk of amputation.[12,13] Bone marrow mesenchymal stem cells (BMSCs) are particularly promising because of their relatively easy accessibility and lack of ethical controversy. They can differentiate into osteoblasts, chondrocytes, adipocytes and myocytes, making them strong candidates for transplantation.[14] Their unique properties, including self-renewal, multipotency, and immunomodulatory capacities, make them complimentary treatments for assisting in neovascularization and tissue regeneration.[15] However, the treatment effectiveness of BMSCs is hindered by their low survival rate in the ischemic microenvironment.[16] Most cells can survive no more than seven days after transplantation.[17] During isolation, digestion, and transplantation, the lifespans of these cells are influenced by multiple factors and processes, including anoikis, in which stem cells undergo apoptosis when separated from the surrounding matrix and neighboring cells.[18] Specific signals or conditions in the micro-environment can trigger stem cell apoptosis.[19,20] Therefore, mitigating anoikis is crucial for improving the survival and function of transplanted cells and enhancing the effectiveness of BMSCs.[21]

Biomaterials have been applied as functional replacements to actively initiate or enhance tissue regeneration.[22] The interactions between biomaterials and cells are emphasized.[23] Unlike traditional chemical materials, biomaterials offer biocompatibility, biodegradability, and tunable functionality, creating a supportive environment resembling the natural extracellular matrix (ECM).[19] Hydrogels are among the most widely accepted biomaterials, forming a 3D network structure that contains large amounts of water.[24] They are commonly made from hydrophilic polymers such as hyaluronic acid, alginate, or chitosan, providing a biocompatible matrix for encapsulating cells.[25] Hydrogels have been used as tissue adhesives and fillers.[26] However, conventional hydrogel materials are not yet ideal therapeutic carriers for cell

delivery because of their low mechanical strength.[27] To address this issue, we synthesized a self-healing hydrogel with good mechanical properties.[28] Furthermore, hydrogels are injectable and can degrade naturally within the body.[29,30]

In addition to the extracellular matrix, oxygen is essential for the survival of stem cells. Ensuring a continuous oxygen supply in a hypoxic environment necessitates a method for sustained oxygen release.[31,32] Oxygen storage and release microspheres, innovative materials, have demonstrated potential in providing effective oxygen supply solutions for biomedical applications.[33,34] Nanospheres, which are nanoscale microspheres that typically range from 1 nm to 1000 nm in size, possess unique physical and chemical properties,[35] including a high specific surface area, high surface energy, and notable optical characteristics attributed to their small size and spherical structure.[36,37] The performance and stability of nanospheres are influenced by factors such as composition, structure, size, and preparation method.[38] Oxygen-releasing nanospheres can provide continuous oxygen during stem cell transplantation, contributing to cell survival, proliferation, and differentiation, as well as repairing damage caused by ischemia and hypoxia.[39] These nanospheres contain storage components that utilize materials with high oxygen adsorption capabilities, such as fluorides, which can enrich oxygen effectively through physical absorption.[40]

Oxygen-releasing nanospheres can supply sufficient oxygen, whereas self-healing hydrogels can provide a supportive environment for stem cells.[41] For effective treatment, biomaterial degradation and tissue regeneration need to be integrated into a delivery system.[42] This study aims to develop an innovative delivery system using oxygen-releasing nanospheres and self-healing hydrogels to increase BMSCs survival and functionality in the treatment of CLTI.

Material and Methods

Nanosphere Synthesis and Characterization

Lecithin (85 mg) was added to 550 μL of Tae's solution and emulsified via a cell crusher (450 W) for 15 minutes (each cycle lasted 8 seconds with 4 seconds interval) in an ice-water bath. The emulsion was added to 450 μL of the original perfluorohexane (PFH) solution at a concentration greater than 97%. The cell crusher was again used to emulsify the mixture for 10 minutes under the same conditions. Oxygen was continuously added to 10% PFH for 30 minutes, and the oxygen-containing emulsion was stored at 4°C until further use.

Next, 0.2 g of chitosan was added to 50 mL of 3% glacial acetic acid solution via magnetic stirring to dissolve 1.5 mL of the oxygenated PFH emulsion. The mixed solution was added to 60 mL of liquid paraffin oil and 5 mL of the surfactant Span-80 and mechanically stirred at 200 rpm for 4 hours in an oil bath at 60°C. The water-oil emulsion was added dropwise to 10 mL of 5% sodium tripolyphosphate (STPP) solution. After the reaction was completed, the emulsion was repeatedly washed with petroleum ether, anhydrous ethanol, and distilled water (5000 rpm for 8 min), lyophilized and set aside.

The rate of oxygen release from nanospheres in different solutions was assessed via an oxygen-sensing probe, and the oxygen release profiles were recorded over time at room temperature (20–24°C).

Assessment of Cell Viability and Cytotoxicity

The viability of the BMSCs cocultured with oxygen-releasing nanospheres was investigated via a cell counting kit-8 (CCK8) viability assay (Yeasen, 40203ES60, China). The cells were seeded in 96-well plates at a density of 5000 cells per well and incubated for 24 hours to allow for adherence and growth. The growth medium was then replaced with fresh medium containing CCK8 reagent, and the plates were incubated for 45 minutes at 37°C. The absorbance at 450 nm was measured via a microplate reader.

An oxidative stress assay was performed to confirm the oxidation-reduction reaction. The cells were seeded in 96-well plates at a density of 50,000 cells per well, treated with an oxidative stress inducer (H_2O_2) for the desired duration, and then incubated with a detection reagent for 30 minutes at room temperature. The fluorescence was measured at 485 nm (excitation) and 535 nm (emission) via a fluorescence microscope.

Hydrogel Synthesis and Characterization

A total of 3.26 g (1.63 mmol) of polyethylene glycol-2000 (PEG2000), 0.98 g (6.52 mmol) of 4-formylbenzoic acid, 0.050 g of 4-dimethylaminopyridine (DMAP), and 1.68 g (8.15 mmol) of dicyclohexylcarbodiimide (DCC) were

dissolved in 100 mL of dry tetrahydrofuran (THF) in a round-bottom flask. The mixture was stirred at 20°C in an oil bath for 18 hours under N_2 protection. After stirring, the mixture was filtered under vacuum, precipitated with precooled ether three times, filtered again, and then dried under vacuum for 24 hours to form benzaldehyde-polyethylene glycol (DF-PEG). 7% hydroxypropyl chitosan (HPCS) granule was dissolved in PBS to form a chitosan solution. Then, 5% DF-PEG was dissolved in PBS to form a solution. These two solutions were mixed at a ratio of 2:1 (7% HPCS: 5% DF-PEG) and allowed to settle in a colloidal state.

The mechanical properties of the hydrogel, including the elastic modulus, tensile strength, and elongation at break, were determined. To observe the morphology of the hydrogels, the swollen hydrogels were frozen in liquid nitrogen and subsequently freeze-dried under vacuum at −20°C for 24 hours. The dry sample was observed by scanning electron microscopy (SEM) (Fei Quan, TA250FEG). The fractured cross-sections were examined via ultra plus field-emission SEM at an accelerating voltage of 15 kV. The sample was sprayed with gold before observation.

For the self-healing capability test, two circular samples were prepared from a mixture of 5% DF-PEG and 7% HPCS, one of which was stained with rhodamine B. Both hydrogel samples were evenly cut into four parts, and the stained and unstained sections were combined. After the samples were left to rest for 24 hours, the fracture interfaces were observed. A shell was used as the mold, and a syringe (1 mL) was injected with DF-PEG solution (rhodamine B stain, 0.3 mL) or HPCS solution (0.6 mL). The hydrogel was sterilized via a 0.22 μm filter membrane to ensure its sterility for in vivo application.

Nanosphere Incorporation

The nanospheres were added into a solution of DF-PEG and thoroughly mixed to ensure even diffusion. The system used in this study was prepared by combining self-healing hydrogels and oxygen-releasing nanospheres under sterile conditions. The composition was optimized to achieve the desired mechanical properties, oxygen release kinetics, and biocompatibility. The nanospheres were carefully analyzed to ensure efficient oxygen release within the hydrogel matrix.

In vivo Cell Coculture with the Delivery System

The cells were labeled with the hydrophilic fluorescent tracer DIR (Yeasen, 40757ES25, China) for in vivo tracking. The excitation spectrum of DIR was close to the near-infrared range (excitation, 748 nm; emission, 780 nm). The dying steps have been described in the previous section. The concentration of the cell-labeling solution was 2.5×10^{-6}/mL. The labeled cells were divided into two groups and mixed with PBS or hydrogel mixture. The labeled cells and nanosphere mixture were incubated at 37°C before the experiment to transform them to a hydrogel state. The mice were anesthetized with isoflurane and injected with 0.06 mL of hydrogel in the left thigh. Differences were detected through a multimodality animal live imaging system (BLT, AV100, China).

Establishment of Lower Limb Ischemia in a Mouse Model

All animals were treated in accordance with the Guidelines for the Nursing and Use of Laboratory Animals, and all experiments were approved by the Ethics Committee of Shanghai Tenth People's Hospital of China (approval number: SHDSYY-2024-1729). Male C57BL/6 mice (6–8 weeks) were obtained from the specific pathogen-free (SPF) Shanghai Tenth People's Hospital Animal Experiment Centre (Shanghai, China). Before all surgical procedures, the mice were anesthetized with pentobarbital sodium (1%, 50 mg/kg, i.p.). Femoral artery ligation and amputation were used to induce CLTI in the mouse model. The mice were depilated at the left thigh, and the femoral artery was separated from the femoral artery sheath. The upper and lower ends of the femoral artery were ligated, and then the vessel in the middle of the ligation was cut. The incision was sutured, and the mice were placed on heat preservation blankets for recovery, which were withdrawn 24 hours later. The state of the mice was observed 3 days after surgery for subsequent experiments.

Assessment of Therapeutic Efficacy

The hydrogel encapsulated with BMSCs was injected intramuscularly into the ischemic limb of the animal model. The therapeutic efficacy was assessed through limb perfusion measurements, enzyme-linked immunosorbent assay (ELISA),

immunohistochemistry, and Masson's trichrome staining. Each group included four mice. In the model of hind limb ischemia induced by unilateral femoral artery ligation, the contralateral hind limb was used as a control. Three days after the limb ischemia operation, the mice were anesthetized with pentobarbital sodium (1%, 50 mg/kg, i.p). The delivery system consisted of 80 $\mu g.mL^{-1}$ nanospheres diffused in 0.3 mL of a mixture of 5% DF-PEG and 7% HPCS in PBS. The BMSCs were loaded in the mixture. The experiment was divided into four groups: normal, ischemia, ischemia treated with BMSCs in PBS and ischemia treated with BMSCs in the delivery system. A 0.3 mL mixture of 6×10^5 BMSCs was injected into the gracilis muscle where ischemia happened with a 26G injection needle. To evaluate the effect of regeneration, the blood perfusion of the hind limbs was continuously monitored by a laser oppler perfusion imaging system (Perimed, NR-PSIN-01228, Sweden) at different time points (0, 1, 2, 3, 4, and 5 weeks) after treatment. The blood flow ratio of the ischemic area was obtained by comparing the blood perfusion intensity of the ischemic area with that of the contralateral unoperated hind limb (limb salvage rate = ischemic limb perfusion rate/contralateral unoperated limb perfusion). After the measurements were taken, the mice were euthanized, and the muscles of the ischemic limb were collected, fixed, and frozen for immunohistochemistry. Similar methods were used for all four groups. To assess fibrosis in muscle tissues, Masson's trichrome staining was performed, and the morphology of the muscle tissue was observed under a microscope (Olympus, BX51, Japan). Immunofluorescence staining of frozen muscle samples was performed to detect the expression of CD31 and α-SMA. A confocal fluorescence microscope (Nikon, Ti-S, Japan) was used for observation and imaging. At least four different randomly stained random fields were counted.

Statistical Analysis

Data analysis was conducted via GraphPad Prism software version 9.5.1 (GraphPad Software, San Diego, USA). Two-tailed Student's *t* tests were used to compare two groups, while multiple comparisons were conducted via one-way analysis of variance (ANOVA). The analytical data are presented as the means ± standard deviations (SDs). Values of $*P < 0.05$, $**P < 0.01$, $*** P < 0.001$, and $****P < 0.0001$ were considered to indicate statistical significance.

Results

Preparation and Characterization of the Delivery System

Preparation of the Delivery System

As previously mentioned, it is difficult for BMSCs to survive in hypoxic environment. To provide a sustainable environment for these stem cells, oxygen-releasing nanospheres and self-healing hydrogels have been developed. Figure 1 illustrates the experimental design and process of creating a novel system composed of nanospheres and hydrogels for delivering BMSCs to a mouse model of limb ischemia. The construction of the oxygen-releasing nanospheres involved several steps. Initially, a PFH emulsion was formed using phosphatidylcholine (Figure 1A and B). Oxygen (O_2) was then introduced into the PFH emulsion to create an oxygenated emulsion. A chitosan solution was subsequently prepared and mixed with acetic acid (Figure 1C). This mixture was heated to form a homogeneous solution. The oxygenated emulsion was combined with sodium tripolyphosphate and processed via a homogenizer to produce oxygen-containing nanospheres (Figure 1D and E). The nanospheres and BMSCs were separately dissolved in the two precursor solutions of the hydrogel (Figure S1). These nanospheres were uniformly dispersed within the hydrogel precursor solution (5% DF-PEG). The BMSCs were subsequently introduced into the other hydrogel precursor solution (7% HPCS). The two solutions were then mixed and immediately injected into the ischemic sites of the lower limbs of the mice (Figure 1F and H). This approach aims to provide a sufficient oxygen supply to BMSCs, thereby enhancing their survival and therapeutic efficacy in the ischemic environment.

Characterization of Oxygen-Releasing Nanospheres

To ensure a consistent oxygen supply for functional BMSCs, oxygen-releasing chitosan nanospheres were developed. These nanospheres cause minimal harm to cells because of their small volume and harmless nature. The nanospheres were obtained through the synthesis of chitosan via an emulsion-solvent evaporation technique, resulting in uniform spherical particles. The surface topology and internal structure of the nanospheres were examined via transmission electron microscopy (TEM), which confirmed their hollow nature and inclusion (Figure 2A–C). Furthermore, the size

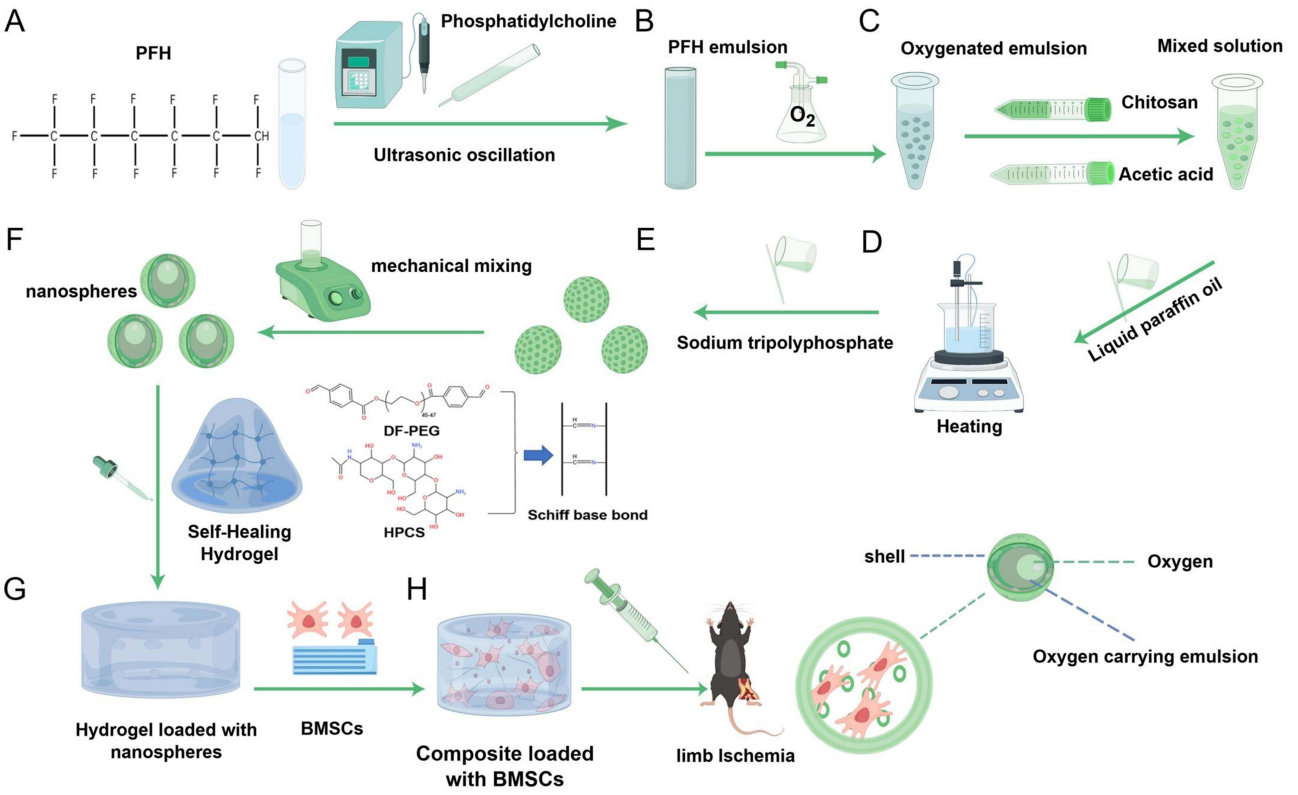

Figure 1 Process of creating and utilizing oxygen-releasing nanospheres and self-healing hydrogels as a delivery system to support BMSCs in the treatment of limb ischemia. The schematic provides a step-by-step illustration of the synthesis and application of oxygen-releasing and self-healing hydrogels loaded with BMSCs for the treatment of limb ischemia. The process is divided into sequential steps labeled (**A**–**H**).

and morphology of the synthesized nanospheres were characterized by scanning electron microscopy (SEM), which revealed a consistent size distribution with an average diameter of approximately 200–300 nm (Figure 2D and E), confirming the uniform size of oxygen-releasing chitosan nanospheres.

To evaluate the oxygen release performance of nanospheres, their oxygen release kinetics were measured under various conditions. Following ultrasonic oscillation, the oxygen content per unit time was measured at 60s, H_2O (1.347 ±0.025) $mg.L^{-1}$, $H_2O(O_2)$ (5.01±0.02) $mg.L^{-1}$ and PFH-CS(O_2) (7.227±0.064) $mg.L^{-1}$ resulted in different release states. Oxygen was completely released at approximately 250 s, H_2O (1.17±0.053) $mg.L^{-1}$ and $H_2O(O_2)$ (1.47±0.01) $mg.L^{-1}$ remain a small amount of oxygen owing to the inability of water to store oxygen. In contrast, PFH-CS(O_2) (6.953 ±0.031) $mg.L^{-1}$, an effective oxygen-carrying emulsion, exhibited slow oxygen release, maintaining high concentrations of O_2 until 900 s, H_2O (0.827±0.021) $mg.L^{-1}$, $H_2O(O_2)$ (1.103±0.015) $mg.L^{-1}$, PFH-CS(O_2) (5.353±0.301) $mg.L^{-1}$, as shown in Figure 2F. When PFH-CS was dissolved in H_2O and PBS, the solution of PFH-CS in PBS resulted in greater and more stable oxygen release. As shown in Figure 2G, 0 $\mu g.mL^{-1}$ (4.126±0.076) $mg.L^{-1}$, 40 $\mu g.mL^{-1}$ (5.043 ±0.33) $mg.L^{-1}$, 80 $\mu g.mL^{-1}$ (5.23±0.403) $mg.L^{-1}$, 120 $\mu g.mL^{-1}$ (4.886±0.26) $mg.L^{-1}$, 160 $\mu g.mL^{-1}$ (5.217±0.079) $mg.L^{-1}$, 200 $\mu g.mL^{-1}$ (4.673±0.23) $mg.L^{-1}$, 240 $\mu g.mL^{-1}$ (4.766±0.209) $mg.L^{-1}$, 280 $\mu g.mL^{-1}$ (4.863±0.102) $mg.L^{-1}$, 320 $\mu g.mL^{-1}$ (5.309±0.224) $mg.L^{-1}$ and 360 $\mu g.mL^{-1}$ (4.636±0.301) $mg.L^{-1}$, different concentrations of nanospheres have different oxygen release abilities. The detection of dissolved oxygen in PBS revealed that concentrations of 40 $mg.L^{-1}$, 80 $mg.L^{-1}$, 160 $mg.L^{-1}$ and 320 $mg.L^{-1}$ nanospheres released more oxygen than the other nanoparticles did (dissolved oxygen above 5 $mg.L^{-1}$). Long-term oxygen release assays were performed with these four concentrations of nanospheres. There was no change of oxygen release in 40 $\mu g.mL^{-1}$ nanospheres after 18 days, indicating oxygen depletion, whereas the other groups still released oxygen. A long-term oxygen release study over 5 weeks revealed that optimal oxygen release was achieved at a concentration of 80 $\mu g.mL^{-1}$, with higher concentrations not resulting in proportionally increased oxygen release. This study confirmed that oxygen-releasing nanospheres provide a reliable and sustained

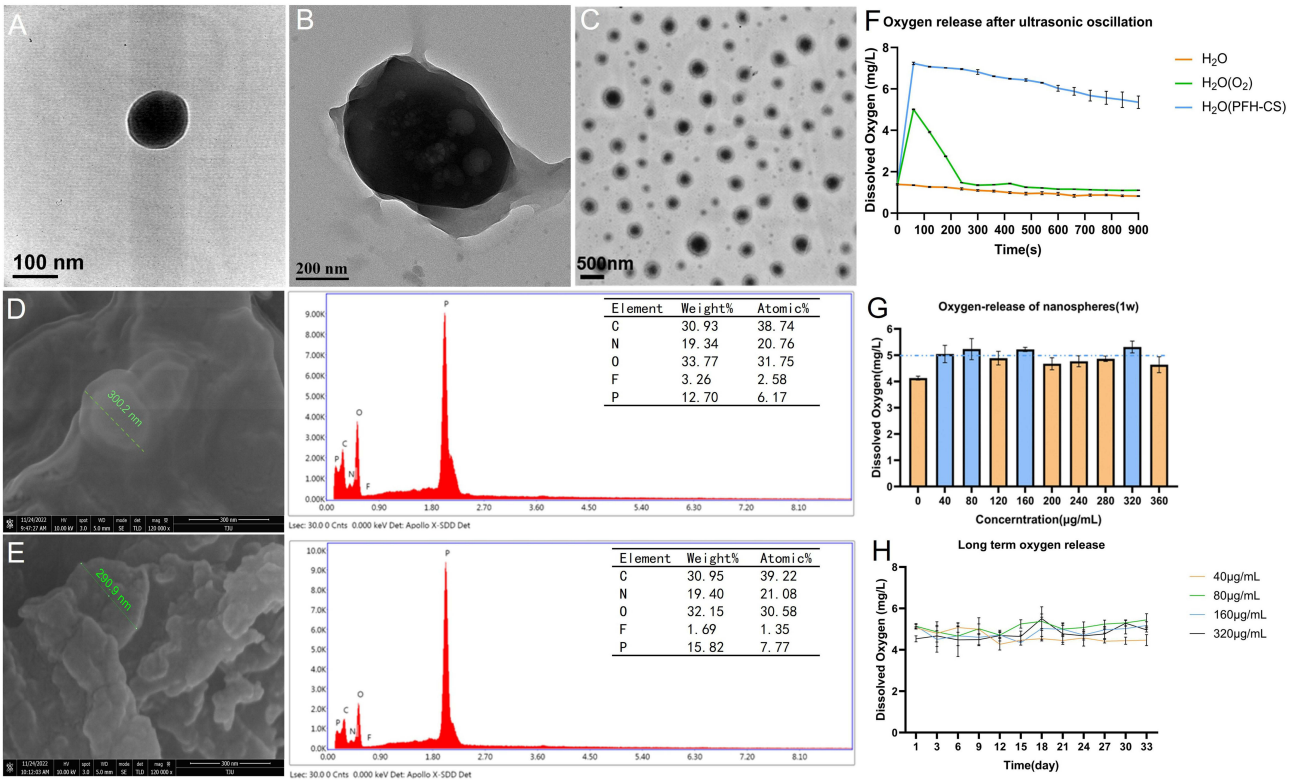

Figure 2 Characterization and oxygen release performance of nanospheres. (**A**) TEM image of a single nanosphere, showing its size and shape. (**B**) TEM image showing a larger view of a nanosphere highlighting the hollow interior structure. (**C**) TEM image of multiple nanospheres displaying a uniform size distribution. (**D**) SEM image of the nanosphere surface with a marked diameter measurement of 300.2 nm. (**E**) SEM image of the nanosphere surface with a marked diameter measurement of 280.9 nm, along with its energy dispersive X-ray spectroscopy (EDX) spectrum showing the elemental composition and corresponding table (C, N, O, F, and P with their weight and atomic percentages). (**F**) Graph showing dissolved oxygen release over time after ultrasonic oscillation in three different solutions: water (H_2O), oxygenated water ($H_2O(O_2)$), and PFH-CS nanospheres diffused in water (H_2O(PFH-CS)). The data are expressed as the means ± SDs (n=4). (**G**) Bar graph representing the oxygen-release capacity of nanospheres after 1 week at different concentrations, showing stable oxygen release across several concentrations. The data are expressed as the means ± SDs (n=7). (**H**) Line graph depicting the long-term oxygen release capacity of nanospheres over a period of 33 days at different concentrations (40 $\mu g.mL^{-1}$, 80 $\mu g.mL^{-1}$, 160 $\mu g.mL^{-1}$, 320 $\mu g.mL^{-1}$), indicating consistent oxygen release over time. The data are expressed as the means ± SDs (n=4).

oxygen supply under various conditions. Over a period of 35 days, the nanospheres showed sustained oxygen release at 40 $\mu g.mL^{-1}$ (4.47±0.263) $mg.L^{-1}$, 80 $\mu g.mL^{-1}$ (5.448±0.303) $mg.L^{-1}$, 160 $\mu g.mL^{-1}$ (5.175±0.176) $mg.L^{-1}$, and 320 $\mu g.mL^{-1}$ (4.965±0.108) $mg.L^{-1}$ at 33 days, indicating a consistent oxygen supply, as shown in Figure 2H. Subsequent experiments were conducted to test 80 $\mu g.mL^{-1}$, 160 $\mu g.mL^{-1}$, 320 $\mu g.mL^{-1}$ of nanospheres.

In vitro Evaluation of Nanosphere Cytotoxicity

Studies of bulk chitosan have shown low cytotoxicity; however, nanoparticles possess unique biological properties, such as high surface-to-area ratio, necessitating new safety evaluations.[43,44] To assess the cytotoxicity of the nanospheres, various concentrations of nanosphere solutions were cocultured with BMSCs (Figure S2A and B). Nanosphere concentrations of 80 $\mu g.mL^{-1}$, 160 $\mu g.mL^{-1}$, and 320 $\mu g.mL^{-1}$ resulted in decreased cell viability (Figure 3A). Notably, coculture with BMSCs mitigated the cytotoxic effects of the nanospheres, suggesting a protective interaction between the BMSCs and the nanospheres. Figure 3B shows that reactive oxygen species (ROS) generation was significantly greater in samples treated with 160 $\mu g.mL^{-1}$ (number of ROS cells, 196±5) and 320 $\mu g.mL^{-1}$ (number of ROS cells, 249±7) than in those treated with 80 $\mu g.mL^{-1}$ (number of ROS cells, 101±2) of nanospheres. The number of cells under oxidative stress (positive control) was 429±5, and the number of cells under oxidative stress (negative control) was 31±2. In addition to the oxidative stress test, cell viability was also assayed via the CCK8 assay, as shown in Figure 3C. After 72 hours, the cell viability of the 80 $\mu g.mL^{-1}$ sample was (156±8)% greater than that of 160 $\mu g.mL^{-1}$ sample (116±5)%, also greater than that of 320 $\mu g.mL^{-1}$ (128±4)%. An 80 $\mu g.mL^{-1}$ nanosphere mixture was selected for further experiments.

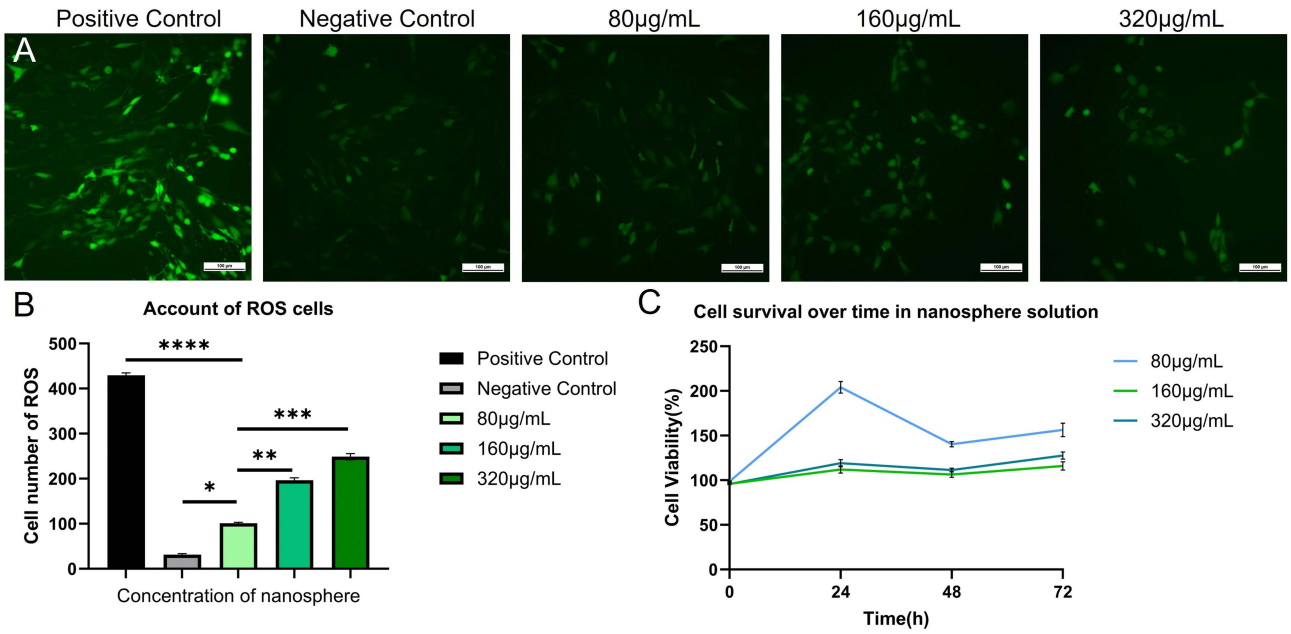

Figure 3 Evaluation of ROS generation and cell viability in nanosphere solutions. (**A**) Representative fluorescence images showing ROS levels in cells under different treatment conditions. (**B**) Bar graph quantifying the number of ROS-positive cells. The data are expressed as the means ± SDs (n = 4). Statistical significance: *$P < 0.05$, **$P < 0.01$, ***$P < 0.001$, ****$P < 0.0001$. (**C**) Line graph depicting cell viability over time for various concentrations of nanosphere solutions. The data are expressed as the means ± SDs (n = 4).

Characterization of the Hydrogels and Combination of Hydrogels and Nanospheres

Characterization of Hydrogels

To synthesize hydrogels with both self-healing properties and suitable mechanical strengths, different solutions of hydrogel components have been implemented, resulting in a three-dimensional network of gelatinous bodies with high water retention capacity (Figure S1B–D), allowing nanospheres to integrate and release oxygen.[45] Photos of SEM revealed the porous structure of the hydrogel (Figure 4A and B). DF-PEG and HPCS were prepared as test samples by pressing potassium bromide and characterized by Fourier transform infrared spectroscopy (FT-IR) in the scanning range of 300–4000 cm^{-1} (Figure 4C). DF-PEG showed a distinct peak at 1724 cm^{-1}, whereas there was no sharp absorption band representing the hydroxyl group in the region of 3700~3200 cm^{-1}, suggesting that polyethylene glycol achieved aldolization. HPCS significantly peaked at both 3451 cm^{-1} and 1645 cm^{-1}, indicating the presence of amide bonding.

Two hydrogel samples, one dyed and one undyed, were evenly cut into two sections and joined together (Figure 4D and E). The fracture junctions bonded after a resting period (Figure 4F). The assembly could be picked up in one piece after 24 hours (Figure 4G), displaying a uniform color indicating the diffusion of components and not breaking by tensile force, demonstrating its self-healing capability.

The mechanical properties of the hydrogels were assessed via injectability tests.[46] Using a seashell as a mold, a low-viscosity hydrogel was injected via a syringe into the designated position (Figure 4H). The fine streams injected into the gaps seamlessly merged, ensuring the macroscopic mechanical properties of the hydrogel and indicating its injectability (Figure 4I), suggesting that the material could conform to complex shapes.[47] Under the action of needle shear, the hydrogel with reduced viscosity could be injected from the syringe to corresponding position (Figure 4J), and the gap between the injected thin streams could be completely fused to ensure the macromechanical properties of the hydrogel (Figure 4K), showing its injectable property with no harm to the cell (Figure S2C). The hydrogel exhibited excellent retention of structural integrity,[48] as evidenced by its ability to form predefined shapes and maintain them without deformation when manipulated with tweezers.[49]

Combination of Hydrogels and Nanospheres

X-ray photoelectron spectroscopy (XPS) revealed that the binding energy of the nanospheres and nanospheres diffused into the hydrogel (Figure 5A). The nanospheres were uniformly incorporated into the hydrogel matrix, as confirmed by

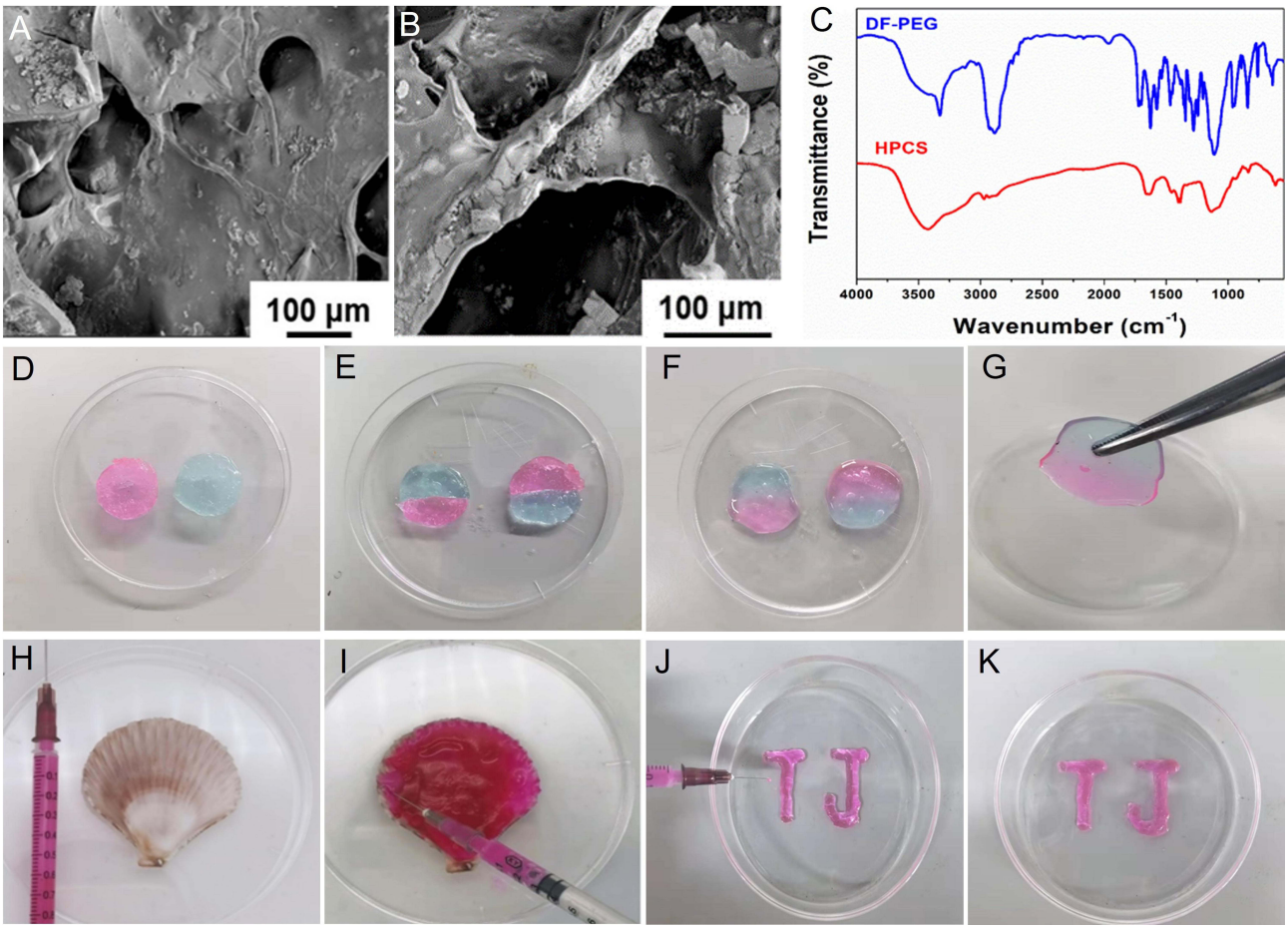

Figure 4 Structural and functional analysis of self-healing hydrogels. (**A** and **B**) SEM images displaying the porous and detailed microstructure of the hydrogels. (**C**) FTIR spectra showing the characteristic peaks of the DF-PEG and HPCS hydrogels. (**D**) Photograph showing two separate colored sections of the hydrogel. (**E**) Hydrogel with two differently colored sections in a Petri dish. (**F**) Hydrogel with merged colored sections, indicating interactions between the sections. (**G**) Image of the hydrogel being manipulated with tweezers, demonstrating its flexibility and mechanical strength. (**H**) A standard syringe and a seashell. (**I**) Injection of a colored solution into the hydrogel, demonstrating its capacity for encapsulation and delivery. (**J**) Photograph showing the formation of the letters "T" and "J" using the hydrogel and a syringe, indicating precise shaping capabilities. (**K**) Image of the letters "T" and "J" formed with the hydrogel, demonstrating post formation of structural integrity.

microstructural analysis. The distribution of nanospheres within the hydrogel was homogeneous, and their stability was evaluated over time; no degradation or leaching from the hydrogel network was detected (Figure 5B).

BMSC Retention in Nanosphere and Hydrogel Delivery Systems

To evaluate the long-term retention of cells, in vivo tracking of labeled BMSCs via bioluminescence imaging was conducted to monitor retention over time (at 3, 6, 12, and 18 days) within the limb tissue. The fluorescence intensity of the BMSCs delivered in PBS rapidly decreased, indicating reduced cell retention over time. On the 18th day, BMSCs in PBS were $1.241^{10}\pm5.558^{8}$ p/s/cm²/sr, BMSCs in hydrogel were $9.965^{9}\pm1.291^{7}$ p/s/cm²/sr, BMSCs in the nanosphere solution were $8.832^{9}\pm5.538^{7}$ p/s/cm²/sr, BMSCs in the hydrogel nanosphere system were $5.655^{10}\pm8.226^{8}$ p/s/cm²/sr ($p=0.0033$). In contrast, the fluorescence intensities of the BMSCs in the hydrogel-nanosphere delivery system were significantly greater at the last time point, indicating improved retention.[50] The delivery system demonstrated the most prolonged retention with detectable signals for up to 18 days, as shown by bioluminescence imaging (Figure 6A).[51] Quantitative analysis of the fluorescence signal confirmed the qualitative imaging results, revealing a clear trend of prolonged retention in the hydrogel-nanosphere system, whereas other conditions resulted in a more rapid decrease in signal intensity (Figure 6B).

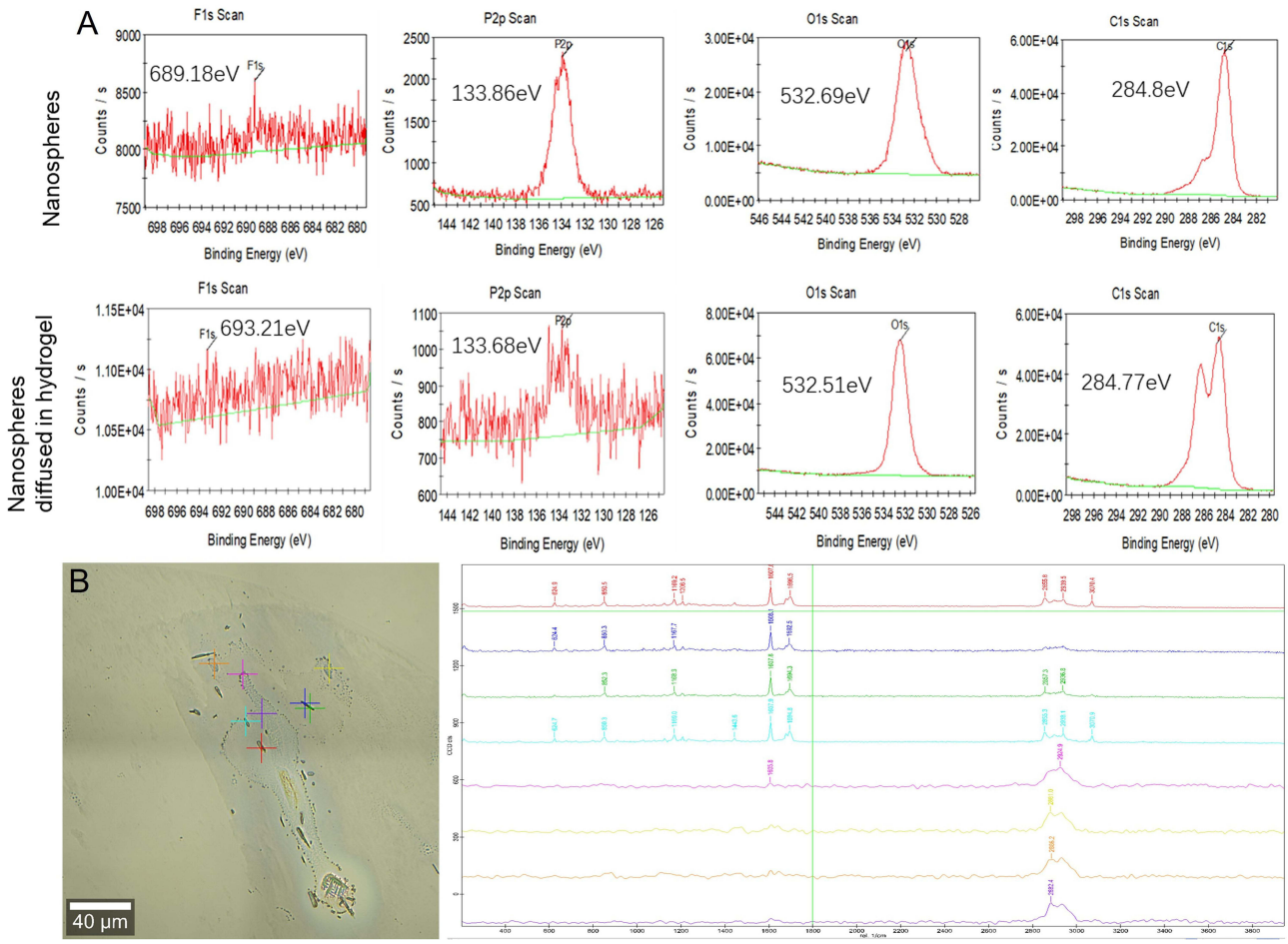

Figure 5 Surface of composition analysis and distribution of nanospheres in hydrogels. (**A**) XPS spectra indicating the binding energies for F1s, P2p, O1s, and C1s in nanospheres before and after diffusion into the hydrogel. The spectra provide insights into the surface composition and chemical states of the elements present. (**B**) Optical microscopy image of the hydrogel with diffuse nanospheres, showing the regions analyzed for elemental distribution. Raman spectrum analysis revealed the spatial distribution and elemental composition of the nanospheres within the hydrogel, highlighting the integration and interaction of the nanospheres with the hydrogel matrix.

Therapeutic Effectiveness of Nanosphere and Hydrogel Delivery Systems in vivo

Revascularization Promotion

Revascularization was evaluated through serial in vivo imaging over 6 weeks. The normal group with a limb salvage rate of (1.076±0.094)% presented stable and high perfusion levels, whereas the ischemic group, with a limb salvage rate of (0.731±0.048)%, presented significantly reduced perfusion. The comparative perfusion levels are illustrated in the thermographic flow images, where the most substantial revascularization was observed in the ischemia group treated with BMSCs in the delivery system group (Figure 7A). During treatment, ischemic limbs treated with BMSCs in the delivery system demonstrated gradual perfusion recovery. Notably, limbs treated with the nanocomposite hydrogel exhibited a more rapid and substantial increase in perfusion as early as the 1st week, with continued improvement over the 6th week. Figure 7B shows the quantification of limb perfusion rates, revealing that ischemic tissue treated with BMSCs in the delivery system group had a limb salvage rate of (0.926±0.024)%, which was significantly greater than that of the BMSCs treatment group, which had a limb salvage rate of (0.841±0.029)%, indicating enhanced vascularization and tissue repair.

Tissue Repair

Immunofluorescence staining revealed the expression of CD31 and α-SMA (Figure S3A and B) in the different treatment groups (Figure 8). The concentrations of vascular endothelial growth factor A (VEGF-A) differed; the normal group (82.674±1.086) pg.mL^{-1}, the ischemia group (65.962±9.947) pg.mL^{-1} ischemia treated with BMSCs (27.462±1.203) pg.

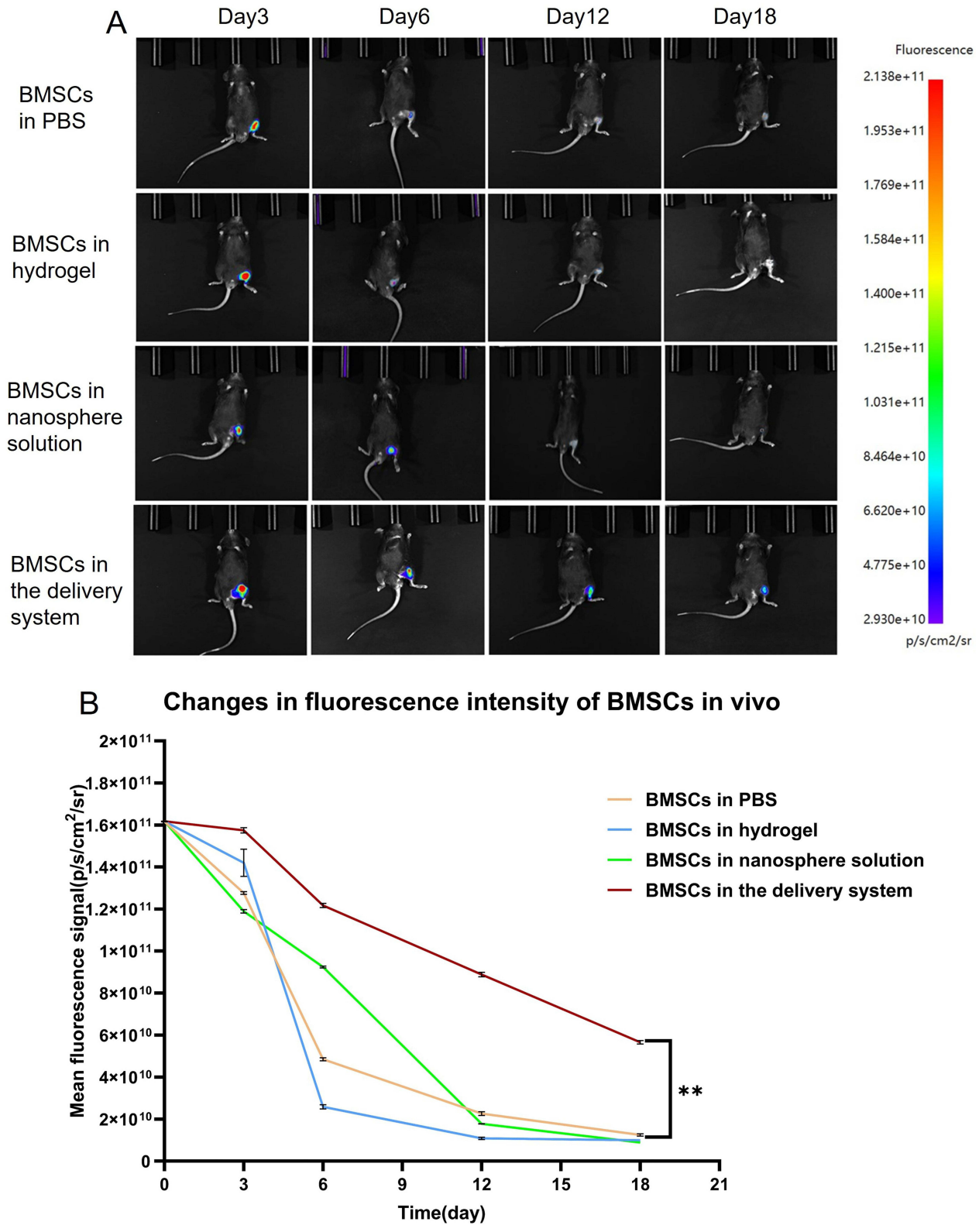

Figure 6 In vivo tracking and fluorescence intensity analysis of BMSCs with different delivery systems. (**A**) In vivo fluorescence images showing the distribution and persistence of BMSCs in mice over time when delivered via phosphate-buffered saline (PBS), a hydrogel, a nanosphere mixture, or a combined delivery system. (**B**) The corresponding graph indicates changes in fluorescence intensity, reflecting the survival and retention of BMSCs in different delivery systems, with the combined delivery system showing the highest retention over 18 days (n=4). Statistical significance: $^{**}P < 0.01$.

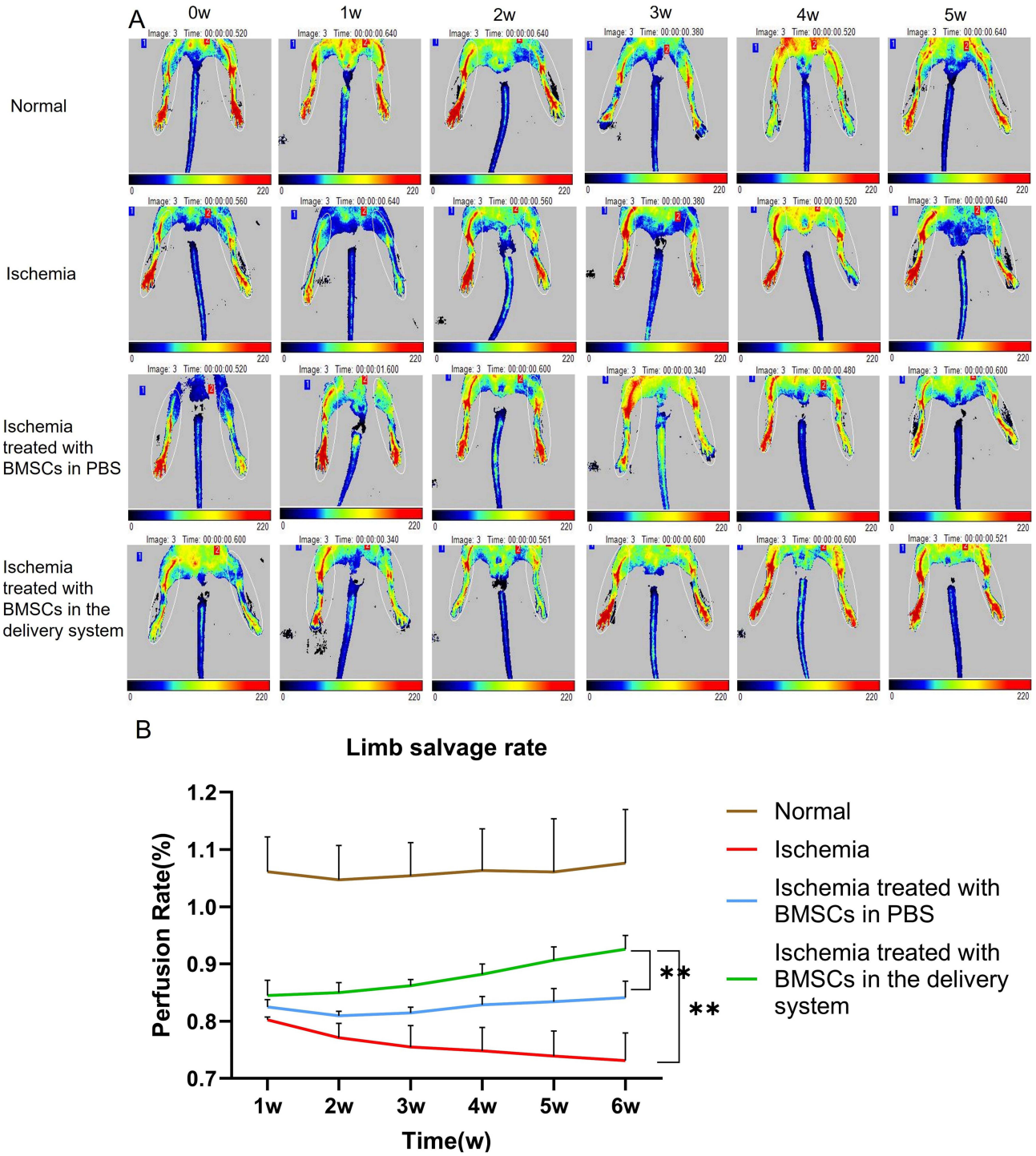

Figure 7 Evaluation of limb perfusion in ischemic tissue treated with BMSCs and the delivery system. (**A**) Laser doppler perfusion images illustrate the changes in limb perfusion over time in normal, ischemic, and treated ischemic tissues. Serial laser Doppler imaging showing blood perfusion levels in the limbs at 0 w, 1 w, 2 w, 3 w, 4 w, 5 w of treatment. The color gradation from dark blue to red indicates the progression from no blood flow to normal blood flow. (**B**) Quantitative analysis of limb salvage rates over 5 weeks post-treatment, represented as a bar graph. Each bar indicates the mean limb salvage rate, with error bars representing the standard deviation. Higher scores denote greater limb rescue rates following treatment. The data are expressed as means ± SDs (n = 4). Statistical significance: $^{**}P < 0.01$.

mL^{-1}, and the ischemia treated with BMSCs (83.379±5.995) $pg.mL^{-1}$ at the 4th week. In the normal group (77.954 ±3.484) $pg.mL^{-1}$, the ischemia group (61.398±5.759) $pg.mL^{-1}$, the ischemia treated with BMSCs group (27.833±2.94) $pg.mL^{-1}$, and the ischemia treated with BMSCs delivery system group (86.893±16.404) $pg.mL^{-1}$ at the 7th week, the expression in ischemic tissue treated with the nanosphere delivery system was greater than that in the other treatment

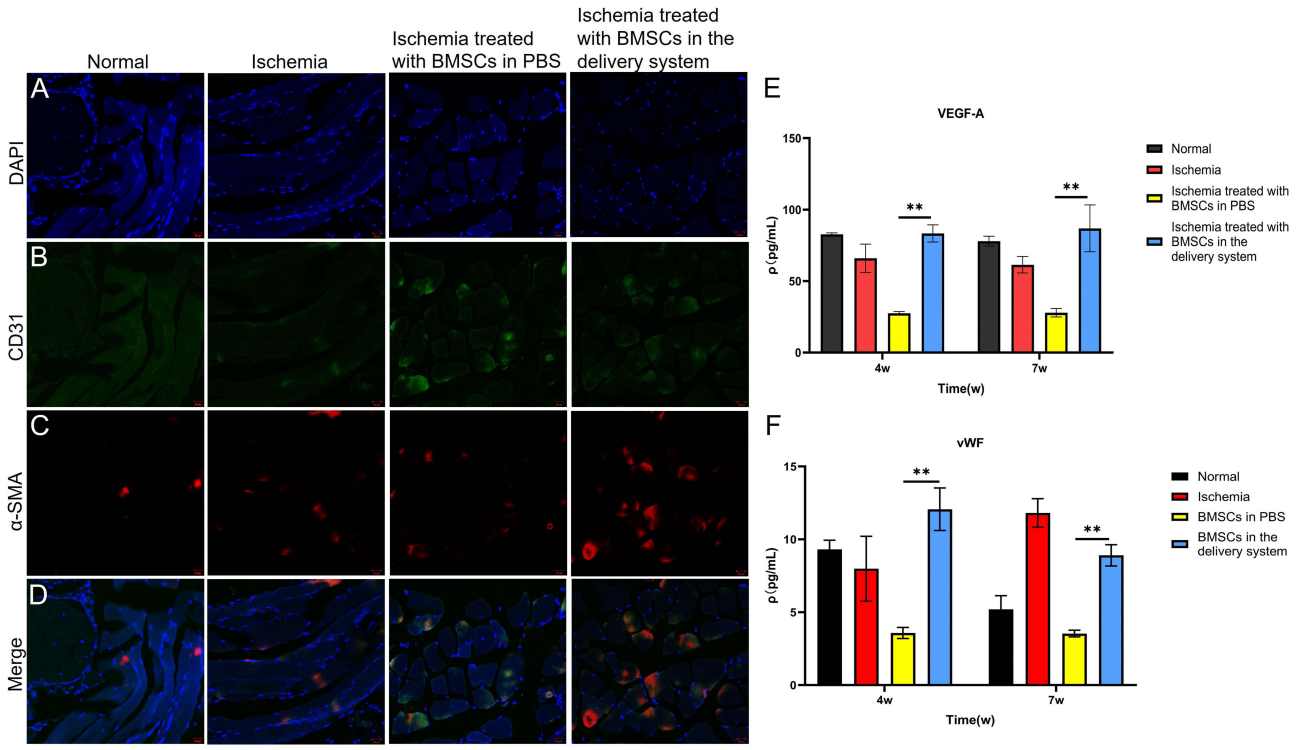

Figure 8 Enhanced angiogenesis and vascularization in ischemic tissue via the delivery of BMSCs via the combined system. Fluorescence microscopy images of BMSCs labeled with CD31 in red and stained for α-smooth muscle actin (α-SMA) in green, under different delivery conditions: BMSCs in phosphate-buffered saline (PBS), BMSCs in hydrogels, and BMSCs in hydrogels with nanosphere solution. The merged images demonstrate the localization, integration, and interaction of BMSCs within the various matrices. Immunofluorescence images of tissue sections showing the expression of angiogenic and vascularization markers in normal, ischemic, and treated ischemic tissues. (**A**) DAPI (blue) for nuclei, (**B**) CD31 (red) for endothelial cells, (**C**) α-SMA (green) represents smooth muscle cells, (**D**) merged images for combined visualization; scale bar = 20 μm. (**E**) The concentration of VEGF-A and (**F**) von Willebrand factor over time, demonstrates enhanced expression in ischemic tissue treated with the nanosphere delivery system compared with other treatments. The data are expressed as means ± SDs (n = 4). Statistical significance: $^{**}P < 0.01$.

groups. The concentrations of von Willebrand factor (vWF) in the 4th week differ; the normal group (9.314±0.628) pg.mL^{-1}, the ischemia group (7.985±2.223) pg.mL^{-1}, the ischemia treated with BMSCs group (3.573±0.38) pg.mL^{-1}, the ischemia treated with BMSCs in the delivery system group (12.066±1.459) pg.mL^{-1}, at the 7th week, normal group (5.202±0.938) pg.mL^{-1}, the ischemia group (11.812±0.98) pg.mL^{-1}, the ischemia treated with BMSCs group (3.534 ±0.23) pg.mL^{-1}, and the ischemia treated with BMSCs in the delivery system (8.902±0.731) pg.mL^{-1}, indicating increased vascularization in the nanosphere delivery systemtreated group, highlighting its efficacy in promoting angiogenesis and tissue repair (Figure S4A-C). A transient increase in cytokines in acute ischemic tissue is beneficial for cell-based therapeutic angiogenesis, enhancing the survival and function of implanted bone marrow cells in the acute limb-threatening ischemic environment.[52]

Antifibrotic Effect

Evaluation of the therapeutic effect of the hydrogel-nanosphere system in limb ischemia via Masson's trichrome staining and immunochemistry (Figure 9A). Temporal series of Masson's trichrome-stained muscle tissue sections from a critical limb ischemia model treated with different therapeutic approaches were analyzed. The staining distinguished muscle fibers (red), connective tissue (blue), and cell nuclei (dark purple), revealing the extent of ischemic damage and the subsequent therapeutic effects of the various treatments over time. Ischemic tissue without treatment, showing extensive muscle damage. Progressive changes in untreated ischemic tissue over 6 weeks, with increasing fibrosis and muscle degradation. Changes in ischemic tissue treated with cells highlighted areas of cell-mediated muscle repair and regeneration. Immunohistochemical analysis revealed that compared with the control group, the treated groups presented reduced fibrosis (Figure S5A and B) and better muscle fiber organization compared to the control group (Figure 9B). Quantitative analysis of TGF-β1 expression (Figure S6A and B) revealed significant differences between normal (0.119±0.007)% and ischemia (0.145±0.003)%, and ischemia treated with BMSCs in PBS

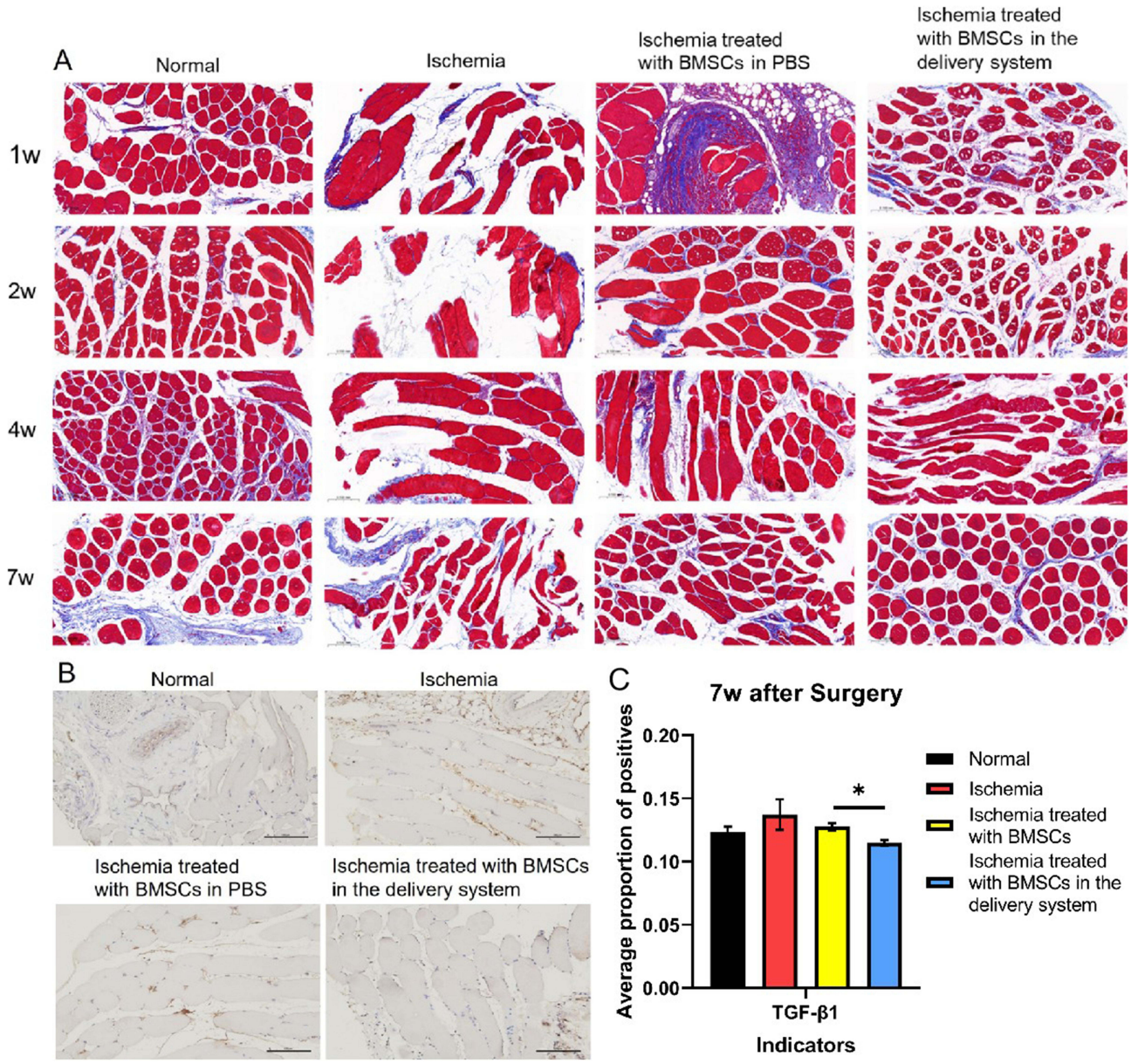

Figure 9 Histological and immunohistochemical analysis of ischemic tissue treated with BMSCs in the delivery system. (**A**) Masson's Trichrome staining of muscle tissue sections at different time points (1 week, 2 weeks, 4 weeks, 7 weeks) under various condition. The staining shows muscle fibers in red and collagen in blue, indicating tissue structure and fibrosis. (**B**) Immunohistochemical staining for inflammatory markers in muscle tissue. Transforming growth factor-beta 1 (TGF-β1) reveals the expression levels of these markers under various conditions, indicating inflammation. Scal bar=100 μm. (**C**) Bar graphs showing the average propotion of positives of TGF-β1 expression in different tissue conditions. The data are expressed as the means ± SDs (n = 4). Statistical significance: *$P < 0.05$.

(0.13±0.002)% and ischemia treated with BMSCs in the delivery system (0.128±0.004)%, highlighting the effectiveness of the nanosphere delivery system in reducing inflammation (Figure 9C). TNF-α and SDF-1α expression also reflects the regulation of inflammation (Figure S6C and D).

Discussion

Lower limb ischemia is categorized into acute, subacute and chronic phases.[53] Although the boundaries between the subacute and chronic phases remain undefined, the period of 7 weeks post-surgery is critical for complementary therapeutic interventions. A major challenge is maintaining stem cell viability for more than 4 weeks. Perfluorocarbons can release oxygen and encapsulate it in chitosan, a natural, non-toxic and biodegradable biomaterial

that enables long-term oxygen release. Oxygen-releasing nanospheres deliver oxygen continuously and maintain a constant release level for up to 35 days, minimizing oxidative stress through controlled dosing.[54]

Supporting cells in the ischemic and hypoxic tissue microenvironments are equally important. Hydrogels, which mimic cellular matrices, are loose, porous, and malleable, making them suitable for loading stem cells and creating a simulated environment for cell culture. In this study, we enhanced the self-healing properties of conventional hydrogels by synthesizing Schiff covalent bonds, allowing the hydrogels to self-heal under ischemic and hypoxic conditions and maintain homeostasis. The biocompatibility, degradability, and non-immunogenicity of chitosan ensure natural degradation in vivo. Future studies should clarify the mechanical properties of hydrogels, such as porosity and pore size, and assess the therapeutic benefits of hydrogel-assisted cell delivery in immunocompetent large animal models.[55]

In vivo imaging confirmed that, compared with BMSCs alone, the hydrogel-nanosphere delivery system significantly prolonged stem cell survival, with fluorescence detectable for up to 18 days. Doppler flowmetry revealed higher perfusion rates in the delivery system group beginning in the 1st week than in the other groups, and the perfusion rates gradually increased and approached normal levels. Immunofluorescence, Masson staining, and enzyme-linked immunosorbent assays revealed that the delivery system treatment group presented new CD31 and α-SMA expression, increased VEGF-A secretion, reduced von Willebrand factor (vWF) secretion, decreased tissue fibrosis, and decreased TGF-β1 levels, reflecting enhanced therapeutic effects.

Our results introduce a novel approach for regulating stem cell activity via the use of new materials, opening new directions for biomaterial-assisted cell therapy.[56] This approach shows promise for clinical translation and therapeutic application.[57] The development of innovative strategies to address the complex challenges of CLTI is crucial.[58] Sustained oxygen release within the hydrogel matrix supports the metabolic demands of BMSCs, increasing their survival.[59] Additionally, the hydrogel serves as a physical barrier, ensuring that BMSCs remain localized at the target tissue, reducing rapid dispersion from the injection site.[60] The oxygen-releasing hydrogels used in our study aimed to increase angiogenesis, regulate inflammation, and inhibit muscle necrosis in patients with lower-limb ischemic diseases.[61]

This study highlights the functionality and efficacy of nanosphere hydrogel systems for controlled oxygen delivery.[62] The system's ability to sustain a prolonged and adaptive oxygen supply under various conditions demonstrates its potential for a wide range of biomedical applications, particularly in treating conditions characterized by poor oxygenation. Future studies should optimize the hydrogel system formulation for specific therapeutic targets and evaluate its in vivo performance to validate its clinical potential.[63] The oxygen-releasing hydrogel delivery system, as an innovative biomedical nanomaterial, continuously releases oxygen, increases tissue oxygen concentrations, improves tissue blood perfusion, oxygenation and tissue repair.[64]

Overall, this therapeutic system is non-toxicity toward cells, significantly prolongs stem cell survival, and markedly enhances the therapeutic efficacy in addressing lower limb ischemia. The mechanism by which the mixture of nanosphere and hydrogel facilitate BMSCs to alleviating ischemia needdiscovering in the following research, involving differentiation of stem cells, to realize more precise regulation. Further validation in larger animal models is needed for clinical application. Future endeavors should prioritize the optimization of the hydrogel system formulations to target specific therapeutic needs and evaluating their long-term performance in larger immunocompetent models.

Conclusion

We have successfully devised a novel delivery system that incorporates oxygen-releasing nanospheres and self-healing hydrogels. This system has been proven to increase stem cell survival and prevent fibrosis, and prevent muscle atrophy in ischemic lower limbs, while efficiently facilitating blood flow reconstruction and recovery. Its therapeutic impact on ischemic diseases is undeniable. After 4 weeks, the system markedly optimized the microenvironment for stem cells, showing substantial therapeutic advantages for chronic limb-threatening ischemia (CLTI) by mitigating fibrosis, augmenting blood flow, enhancing tissue perfusion, and fostering angiogenesis and tissue recovery.

In summary, our research underscores high potential of this innovative delivery system in addressing ischemic conditions, offering a promising avenue for bridging the gaps in existing therapeutic strategies.

Abbreviations

PFH-CS, perfluorohexane-chitosan; DIR, 1.1-dioctadecyl-3,3,3,3-tetramethylindotricarbocyaine iodide; ROS, reactive oxygen species; PBS, phosphate-buffered saline; BMSC, mouse bone marrow mesenchymal stem cell; α-SMA, alpha-smooth muscle actin; H&E, hematoxylin and eosin; TGF-β1, transforming growth factor-beta 1; TNF-α, tumor necrosis factor-alpha; SDF-1α, stromal cell-derived factor 1-alpha; DAPI, 4',6-diamidino-2-phenylindole; CD31, Platelet endothelial cell adhesion molecule-1; TEM, transmission electron microscope; SEM, scanning electron microscopy.

Acknowledgments

This work was supported by the National Natural Science Foundation of China (Grant no. 8207070257). BMSCs cell line (#MUBMX-01001, OriCell^{TM}) was purchased from Cyagen Biosciences (GuangZhou) Inc, China for experimental use.

Disclosure

The authors report no conflicts of interest in this work.

References

1. Cedric S, vdL L, Nick S, Anne M, Inge F. Chronic Limb-Threatening Ischemia does not Enclose a Homogenous Population: time for a More Detailed Classification. *Int J Angiology*. 2024;33(01):8–14. doi:10.1055/s-0043-1777414
2. Armstrong EJ. Intensifying our focus on critical limb ischemia. *Vasc Med*. 2021;26(2):121–122. doi:10.1177/1358863X211000425
3. Choi JC-B, Miranda J, Greenleaf E, et al. Lower-extremity pressure, staging, and grading thresholds to identify chronic limb-threatening ischemia. *Vascular Medicine*. 2023;28(1):45–53. doi:10.1177/1358863X221147945
4. Chu D, Zheng X, Mao J, Ramsey L, Mukherjee D. Comparison of endovascular therapies for chronic limb-threatening ischemia and claudication. *J Vascular Surg*. 2024;79(4):875–886.e8. doi:10.1016/j.jvs.2023.12.001
5. Campbell DB, Sobol CG, Sarac TP, Stacy MR, Atway S, Go MR. The natural history of chronic limb-threatening ischemia after technical failure of endovascular intervention. *J Vascular Surg*. 2023;78(3):737–744. doi:10.1016/j.jvs.2023.04.034
6. Panel P, Abramson BL, Al-Omran M, et al. Canadian Cardiovascular Society 2022 Guidelines for Peripheral Arterial Disease. *Can. J Cardiol*. 2022;38(5):560–587.
7. Kutsenko O, Sommerset J, Chandra V, Bryce Y. Techniques Providing Endpoints for Revascularization in Chronic Limb-Threatening Ischemia. *Semin Interventi Radiology Apr*. 2023;40(02):177–182. doi:10.1055/s-0043-1768608
8. Karimi A, Lauria AL, Aryavand B, Neville RF. Novel Therapies for Critical Limb-Threatening Ischemia. *Curr Cardiol Rep*. 2022;24(5):513–517. doi:10.1007/s11886-022-01669-6
9. Husakova J, Bem R, Jirkovska A, et al. Comparison of Three Methods for Preparation of Autologous Cells for Use in Cell Therapy of Chronic Limb-Threatening Ischemia in People with Diabetes. *Int J Low Extrem Woun*.
10. Arango-Rodríguez ML, Mateus LC, Sossa CL, et al. A novel therapeutic management for diabetes patients with chronic limb-threatening ischemia: comparison of autologous bone marrow mononuclear cells versus allogenic Wharton jelly-derived mesenchymal stem cells. *Stem Cell Res Ther*. 2023;14(1):221. doi:10.1186/s13287-023-03427-z
11. Nakamoto Y, Nakamura T, Nakai R, Azuma T, Omori K. Transplantation of autologous bone marrow-derived mononuclear cells into cerebrospinal fluid in a canine model of spinal cord injury. *Regen Ther*. 2023;24:574–581. doi:10.1016/j.reth.2023.10.003
12. Krafcik B, Goodney PP. Trust and Time Matter When Treating Chronic Limb-Threatening Ischemia. *JAMA Surg*. 2023;158(6):e230487. doi:10.1001/jamasurg.2023.0487
13. Lozano Navarro LV, Chen X, Giratá Viviescas LT, et al. Mesenchymal stem cells for critical limb ischemia: their function, mechanism, and therapeutic potential. *Stem Cell Res Ther*. 2022;13(1):345. doi:10.1186/s13287-022-03043-3
14. Asadi-Yousefabad SL, Nammian P, Sheikhha MH, et al. Comparative study of mouse adipose- and bone marrow mesenchymal stem cells in diabetic model with critical limb ischemia. *Cell Tissue Bank*. 2022;23(4):923–936. doi:10.1007/s10561-022-10007-7
15. Lee S, Choi E, Cha MJ, Hwang KC. Cell adhesion and long-term survival of transplanted mesenchymal stem cells: a prerequisite for cell therapy. *Oxid Med Cell Longev*. 2015;2015:632902. doi:10.1155/2015/632902
16. Delanois RE, Sax OC, Chen Z, Cohen JM, Callahan DM, Mont MA. Biologic Therapies for the Treatment of Knee Osteoarthritis: an Updated Systematic Review. *J Arthroplasty*. 2022;37(12):2480–2506. doi:10.1016/j.arth.2022.05.031
17. Ortega MA, De Leon-Oliva D, Boaru DL, et al. Unraveling the New Perspectives on Antimicrobial Hydrogels: state-of-The-Art and Translational Applications. *Gels*. 2023;9(8):617. doi:10.3390/gels9080617
18. Zhang T, Zhang Q, Yu WC. Mammalian Ste20-like kinase 1 inhibition as a cellular mediator of anoikis in mouse bone marrow mesenchymal stem cells. *World. J Stem Cells*. 2023;15(3):90–104.
19. Luo S, Wu J, Qiu Y, et al. Hydrogen Promotes the Effectiveness of Bone Mesenchymal Stem Cell Transplantation in Rats with Spinal Cord Injury. *Stem Cells Int*. 2023;2023:8227382. doi:10.1155/2023/8227382
20. Li X, Li X, Yang J, et al. Living and Injectable Porous Hydrogel Microsphere with Paracrine Activity for Cartilage Regeneration. *Small*. 2023;19(17):e2207211. doi:10.1002/smll.202207211
21. Caliari SR, Burdick JA. A practical guide to hydrogels for cell culture. *Review Nature Methods*. 2016;13(5):405–414. doi:10.1038/nmeth.3839
22. Daghrery A, Bottino MC. Advanced biomaterials for periodontal tissue regeneration. *Genesis*. 2022;60(8–9):e23501. doi:10.1002/dvg.23501
23. Liu Z, Wan X, Wang ZL, Li L. Electroactive Biomaterials and Systems for Cell Fate Determination and Tissue Regeneration. *Desi Applic Adv Mater*. 2021;33(32):e2007429.

24. Barcena AJR, Dhal K, Patel P, Ravi P, Kundu S, Tappa K. Current Biomedical Applications of 3D-Printed Hydrogels. *Gels*. 2023;10(1):8. doi:10.3390/gels10010008
25. Al Mamun A, Ullah A, Chowdhury MEH, et al. Oxygen releasing patches based on carbohydrate polymer and protein hydrogels for diabetic wound healing: a review. *Int J Biol Macromol*. 2023;250:126174. doi:10.1016/j.ijbiomac.2023.126174
26. Atila D, Kumaravel V. Advances in antimicrobial hydrogels for dental tissue engineering: regenerative strategies for endodontics and periodontics. *Biomater Sci*. 2023;11(20):6711–6747. doi:10.1039/D3BM00719G
27. Cai R, Shan Y, Du F, et al. Injectable hydrogels as promising in situ therapeutic platform for cartilage tissue engineering. *Int J Biol Macromol*. 2024;261(Pt1):129537. doi:10.1016/j.ijbiomac.2024.129537
28. Huang W, Wang Y, Chen Y, et al. Strong and Rapidly Self-Healing Hydrogels: potential Hemostatic Materials. *Adv Healthc Mater*. 2016;5 (21):2813–2822. doi:10.1002/adhm.201600720
29. Li Q, Zhang S, Du R, et al. Injectable Self-Healing Adhesive Natural Glycyrrhizic Acid Bioactive Hydrogel for Bacteria-Infected Wound Healing. *ACS Appl Mate Inter*. 2023;15(14):17562–17576. doi:10.1021/acsami.2c23231
30. Li Y, Yang D, Wu Z, et al. Self-adhesive, self-healing, biocompatible and conductive polyacrylamide nanocomposite hydrogels for reliable strain and pressure sensors. *Nano Energy*. 2023;109108324.
31. Bai Q, Zheng C, Sun N, et al. Oxygen-releasing hydrogels promote burn healing under hypoxic conditions. *Acta Biomater*. 2022;154:231–243. doi:10.1016/j.actbio.2022.09.077
32. Patenaude R, Yasmin-Karim S, Peng Y, et al. Injectable Oxygen Microparticles Boost Radiation-Mediated In Situ Vaccination and Systemic Antitumor Immune Responses. *Int J Radiat Oncol Biol Phys*. 2023;116(4):906–915. doi:10.1016/j.ijrobp.2022.12.051
33. Hosseini FS, Abedini AA, Chen F, Whitfield T, Ude CC, Laurencin CT. Oxygen-Generating Biomaterials for Translational Bone Regenerative Engineering. *ACS Appl Mater Interf*. doi:10.1021/acsami.2c20715
34. Suvarnapathaki S, Nguyen A, Goulopoulos A, Camci-Unal G. Oxygen-Generating Scaffolds for Cardiac Tissue Engineering Applications. *ACS. Biomater Sci Eng*. 2023;9(1):409–426. doi:10.1021/acsbiomaterials.2c00853
35. Hassan F, Tang Y, Bisoyi HK, Li Q. Photochromic Carbon Nanomaterials: an Emerging Class of Light-Driven Hybrid Functional Materials. *Adv Mater*.
36. Li Y, Dang G, Rizwan Younis M, et al. Peptide functionalized actively targeted MoS2 nanospheres for fluorescence imaging-guided controllable pH-responsive drug delivery and collaborative chemo/photodynamic therapy. *J Colloid Interface Sci*. 2023;639:302–313. doi:10.1016/j.jcis.2023.02.027
37. Lu T, Deng X, Sun Q, et al. 3D Carbiyne Nanospheres Boosting Excellent Lithium and Sodium Storage Performance. *Small*. 2022;18(3):e2106328. doi:10.1002/smll.202106328
38. Zhao J, Ma Z, Qiao C, Fan Y, Qin X, Shao G. Spectroscopic Monitoring of the Electrode Process of MnO_2@rGO Nanospheres and Its Application in High-Performance Flexible Micro-Supercapacitors. *ACS Appl Mater Interf*. 2022;14(30):34686–34696. doi:10.1021/acsami.2c06850
39. Chen Z, Niu M, Chen G, et al. Oxygen Production of Modified Core-Shell CuO@ZrO2 Nanocomposites by Microwave Radiation to Alleviate Cancer Hypoxia for Enhanced Chemo-Microwave Thermal Therapy. *ACS Nano*. 2018;12(12):12721–12732. doi:10.1021/acsnano.8b07749
40. Lu Y, Han X, Zhang Y, Yu X. Graphene Architecture-Supported Porous Cobalt-Iron Fluoride Nanosheets for Promoting the Oxygen Evolution Reaction. *Nanomaterials*.
41. Guan Y, Gao N, Niu H, Dang Y, Guan J. Oxygen-release microspheres capable of releasing oxygen in response to environmental oxygen level to improve stem cell survival and tissue regeneration in ischemic hindlimbs. *J Control Release*. 2021;331:376–389. doi:10.1016/j.jconrel.2021.01.034
42. Hu J, Xu Z, Liao D, et al. An H_2 S-BMP6 Dual-Loading System with Regulating Yap/Taz and Jun Pathway for Synergistic Critical Limb Ischemia Salvaging Therapy. *Adv Healthc Mater*. 2023;12(28):e2301316. doi:10.1002/adhm.202301316
43. Abdelazim K, Ghit A, Assal D, et al. Production and therapeutic use of astaxanthin in the nanotechnology era. *Pharmacol Rep*. 2023;75 (4):771–790. doi:10.1007/s43440-023-00488-y
44. Ahmed TA, Aljaeid BM. Preparation, characterization, and potential application of chitosan, chitosan derivatives, and chitosan metal nanoparticles in pharmaceutical drug delivery. *Drug Des Devel Ther*. 2016;10:483–507. doi:10.2147/DDDT.S99651
45. Wang L, Zhao Z, Dong J, et al. Mussel-Inspired Multifunctional Hydrogels with Adhesive, Self-Healing, Antioxidative, and Antibacterial Activity for Wound Healing. *ACS Appl Mater Interf*. 2023;15(13):16515–16525. doi:10.1021/acsami.3c01065
46. Wang C, Liu Y, Qu X, et al. Ultra-Stretchable and Fast Self-Healing Ionic Hydrogel in Cryogenic Environments for Artificial Nerve Fiber. *Adv Mater*. 2022;34(16):e2105416. doi:10.1002/adma.202105416
47. Guo S, Ren Y, Chang R, et al. Injectable Self-Healing Adhesive Chitosan Hydrogel with Antioxidative, Antibacterial, and Hemostatic Activities for Rapid Hemostasis and Skin Wound Healing. *ACS Appl Mater Interf*. 2022;14(30):34455–34469. doi:10.1021/acsami.2c08870
48. Feng W, Wang Z. Shear-thinning and self-healing chitosan-graphene oxide hydrogel for hemostasis and wound healing. *Carbohydr Polym*. 2022;294:119824. doi:10.1016/j.carbpol.2022.119824
49. Bai Q, Gao Q, Hu F, et al. Chitosan and hyaluronic-based hydrogels could promote the infected wound healing. *Int J Biol Macromol*. 2023;232:123271. doi:10.1016/j.ijbiomac.2023.123271
50. Chen LM, Zheng BR, Xu YZ, et al. Nano hydrogel-based oxygen-releasing stem cell transplantation system for treating diabetic foot. *J Nanobiotechnol*. 2023;21(1):13.202. doi:10.1186/s12951-023-01925-z
51. Zhong T, Gao N, Guan Y, Liu Z, Guan J. Co-Delivery of Bioengineered Exosomes and Oxygen for Treating Critical Limb Ischemia in Diabetic Mice. *ACS Nano*. 2023;17(24):25157–25174. doi:10.1021/acsnano.3c08088
52. Qin SL, Li TS, Kubo M, Ohshima M, Furutani A, Hamano K. Transient increase of cytokines in the acute ischemic tissue is beneficial to cell-based therapeutic angiogenesis. *Circ J*. 2008;72(12):2075–2080. doi:10.1253/circj.CJ-08-0392
53. Gray BH, Wheibe E, Dicks AB, Low ML, Tingen JS. Pounce Thrombectomy System to Treat Acute and Chronic Peripheral Arterial Occlusions. *Ann Vasc Surg*. 2023;96:104–114. doi:10.1016/j.avsg.2023.05.019
54. Zhu Q, Hao H, Xu H, et al. Combination of Antioxidant Enzyme Overexpression and N-Acetylcysteine Treatment Enhances the Survival of Bone Marrow Mesenchymal Stromal Cells in Ischemic Limb in Mice With Type 2 Diabetes. *J Am Heart Assoc*. 2021;10(19):e023491. doi:10.1161/JAHA.121.023491
55. Bialas F, Reichinger D, Becker CFW. Biomimetic and biopolymer-based enzyme encapsulation. *Enzyme Microb Technol*. 2021;150:109864. doi:10.1016/j.enzmictec.2021.109864

56. Huerta CT, Voza FA, Ortiz YY, Liu ZJ, Velazquez OC. Mesenchymal stem cell-based therapy for non-healing wounds due to chronic limb-threatening ischemia: a review of preclinical and clinical studies. *Front Cardiovasc Med*. 2023;10:1113982. doi:10.3389/fcvm.2023.1113982
57. Huerta CT, Voza FA, Ortiz YY, Liu ZJ, Velazquez OC. Targeted cell delivery of mesenchymal stem cell therapy for cardiovascular disease applications: a review of preclinical advancements. *Front Cardiovasc Med*. 2023;10:1236345. doi:10.3389/fcvm.2023.1236345
58. Setia O, Lee S-R, Dardik A. Modalities to Deliver Cell Therapy for Treatment of Chronic Limb Threatening Ischemia. *Adv Wound Care*. 2024;13 (5):253–279. doi:10.1089/wound.2022.0114
59. Xing Z, Zhao C, Wu S, Zhang C, Liu H, Fan Y. Hydrogel-based therapeutic angiogenesis: an alternative treatment strategy for critical limb ischemia. *Biomaterials*. 2021;274:120872. doi:10.1016/j.biomaterials.2021.120872
60. Lakshmanan R, Ukani G, Rishi MT, Maulik N. Trimodal rescue of hind limb ischemia with growth factors, cells, and nanocarriers: fundamentals to clinical trials. *Can J Physiol Pharmacol*. 2017;95(10):1125–1140. doi:10.1139/cjpp-2016-0713
61. Yuan Y, Zhang Z, Mo F, et al. A biomaterial-based therapy for lower limb ischemia using Sr/Si bioactive hydrogel that inhibits skeletal muscle necrosis and enhances angiogenesis. *Bioact Mater*. 2023;26:264–278. doi:10.1016/j.bioactmat.2023.02.027
62. Bhatt P, Pandey SC, Joshi S, et al. Nanobioremediation: a sustainable approach for the removal of toxic pollutants from the environment. *J Hazard Mater*. 2022;427:128033. doi:10.1016/j.jhazmat.2021.128033
63. Lv Y, Cai F, He Y, et al. Multi-crosslinked hydrogels with strong wet adhesion, self-healing, antibacterial property, reactive oxygen species scavenging activity, and on-demand removability for seawater-immersed wound healing. *Acta Biomater*. 2023;159:95–110. doi:10.1016/j.actbio.2023.01.045
64. Li S, Dong Q, Peng X, et al. Self-Healing Hyaluronic Acid Nanocomposite Hydrogels with Platelet-Rich Plasma Impregnated for Skin Regeneration. *ACS Nano*. 2022;16(7):11346–11359. doi:10.1021/acsnano.2c05069